FEBS Letters 585 (2011) 485–491

FEBS Letters

journal homepage: www.FEBSLetters.org

Cis–trans isomerization of the Epstein–Barr virus determinant peptide EENLLDFVRF after the DM1 TCR recognition of the HLA-B*4405/peptide complex

Athanassios Stavrakoudis *

Department of Economics, University of Ioannina, GR-451 10 Ioannina, Greece

ARTICLE INFO

Article history:
Received 18 August 2010
Revised 23 November 2010
Accepted 8 December 2010
Available online 15 December 2010

Edited by Robert B. Russell

Keywords:
Cis–trans peptide isomerization
Class I MHC
Epstein–Barr virus nuclear antigen
HLA-B44
Molecular dynamics
Peptide/MHC/TCR interactions

ABSTRACT

The Epstein–Barr virus determinant peptide EENLLDFVRF shows high immunogenicity when presented by HLA-B*4405 allotype. This fact is accompanied by a *cis–trans* isomerization of the Leu5-Asp6 peptide bond upon TCR binding of the pMHC complex. Molecular dynamics simulations of pMHC/TCR structures, with the EENLLDFVRF peptide in *cis* and *trans* conformations have been employed in order to examine the structure and dynamics of the pMHC complex with such an unusual conformation. The results, based on MM-PBSA free energy computations as well as buried surface area analysis and interactions at the pMHC/TCR interface, indicate that the TCR binds preferably the pMHC complex with the Leu5-Asp6 peptide bond in *cis* conformation. It is the first time that this notable conformational feature of T-cell epitope is investigated.

1. Introduction

Flexibility in peptide binding by protein receptors is a well known issue [1]. Targeting this feature of peptides conformation in immunological complexes can have significant impact in designing successful vaccines [2]. *Cis–trans* isomerization has been observed mainly in proline residues in proteins [3,4], although it can be found in other residues as well [5]. The pore functionality of a neurotransmitter-gated ion channel at Cys-loop receptor super-family is a classical paradigm of how *cis–trans* isomerization can affect biological binding and activity [6]. In small peptides, *cis–trans* isomerization can be influenced by specific side chain interactions [7], while in proteins it can be modulated by enzymatic action [8]. *Cis–trans* isomerization has been observed in both B-cell epitopes [9,10] and T-cell epitopes in peptide/MHC complexes [11]. It has been noted that *cis–trans* isomerization must be carefully taken into account in predicting peptide conformations bound to the major histo-compatibility complex (MHC) molecules [12].

Recently, the X-ray structure of the Epstein–Barr virus determinant peptide, with sequence E^{1}ENLLDFVRF^{10}, bound to HLA-B*4405 molecule (pMHC complex) has been determined [13], along with the X-ray structure of the pMHC complexed with DM1 T-cell receptor (TCR). The authors compared the X-ray structure of HLA-B*4405$^{\text{EENLLDFVRF}}$ with HLA-B*4402$^{\text{EENLLDFVRF}}$ and HLA-B*4403$^{\text{EENLLDFVRF}}$ X-ray structures and concluded that peptide flexibility was critical in preferential engagement with HLA-B*4405 in comparison to HLA-B*4402/03, resulting in finetuning of T cell responses between closely related allotypes. One striking feature of the peptide's conformation in pMHC/TCR complex was the adoption of *cis* isomerization state in Leu5-Asp6 peptide bond, while the same bond was found in *trans* isomerization state in the pMHC complex.

The rules by which the TCRs interact with pMHC complexes are not yet clearly understood [14,15], but there is a continuous increase in our knowledge as more pMHC/TCR complexes appear in the Protein Data Bank. Currently, there is no other example described in the literature with peptide in pMHC/TCR complex possessing a *cis* peptide bond, after the formation of pMHC/TCR complex. Of course, *cis–trans* isomerization might not be considered a global feature of peptide structure in pMHC/TCR complexes, and this observation cannot be generalized in all pMHC/TCR complexes. However, the case described here is notable, as it is seen in biological affinity experiments [13].

Molecular dynamics simulations have been extensively used in immunological and pharmaceutical research during past years [16,17]. It has been argued that this approach can augment our knowledge gained from experimental research [18,19]. Thus, extensive molecular dynamics studies of pMHC/TCR complexes are presented here, with the aim to explore the dynamic properties

* Fax: +30 265 100 5092.
E-mail address: astavrak@cc.uoi.gr
URL: http://stavrakoudis.econ.uoi.gr

0014-5793/$36.00
doi:10.1016/j.febslet.2010.12.013

of the peptide's conformations in the two complexes and to explain why the TCR prefers to bind a pMHC complex with a peptide in *cis* conformation.

2. Methods

2.1. System setup and simulation

Initial coordinates the TCR–HLA-B*4405^{EENLLDFVRF} complex were downloaded from Protein Data Bank [20], access code 3dxa [13]. In this structure, the ω dihedral angle between Leu5 and Asp6 residues is found 16.6°, thus in *cis* conformation. This complex will be referred as TCR–HLA^{cpep} hereafter. Another complex, with the peptide in *trans* conformation was also modeled in this study. The peptide structure from the HLA-B*4405–peptide complex (TCR free complex) was extracted and its coordinates were superimposed onto the coordinates of the peptide in the TCR–HLA^{cpep} complex. These coordinates were taken from the PDB structure 3dx8 [13], where the peptide lies in the *trans* conformation. The rest of the molecular complex (MHC + TCR) was left untouched.

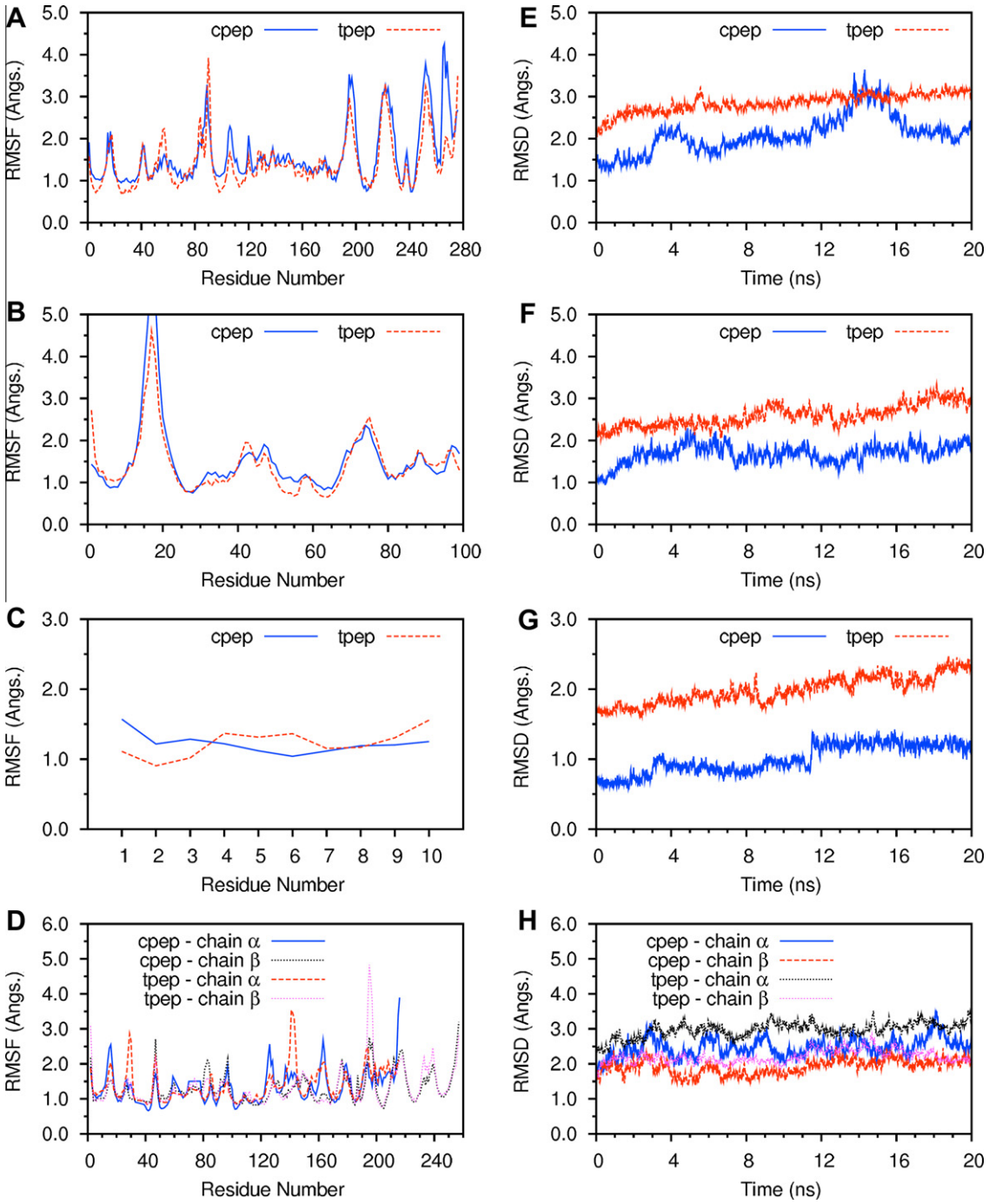

Fig. 1. Root mean square fluctuation (RMSF) of C^{α} atoms and root mean square deviation (RMSD) time series of backbone atoms (N, C^{α}, C) after fitting the corresponding atom positions from MD trajectories to the initial coordinates. Results from different trajectories (TCR–HLA^{cpep} and TCR–HLA^{cpep}) are indicated with different line colors and styles. (A) RMSF of C^{α} atoms of MHC chain α, (B) RMSF of C^{α} atoms of MHC chain β, (C) RMSF of C^{α} atoms of the peptide, (D) RMSF of C^{α} atoms of chains α, β (D,E) of DM1 TCR, (E) RMSD of backbone atoms of MHC chain α, (F) RMSD of backbone atoms of MHC chain β, (G) RMSD of backbone atoms of the peptide, (H) RMSD of backbone atoms of the TCR's chains α and β, respectively (D,E).

This complex will be referred as TCR–HLA^{tpep} hereafter. Both complexes were treated under exactly the same simulation protocol.

Topology and force field parameters for all atoms were assigned from the CHARMM27 parameter set [21]. Hydrogen atoms were added with the VMD program [22] and its autopsf utility. Protonation status of Histidine side chains was determined with the REDUCE program [23]. The protein complexes was centered in a rectangular box with dimensions 87.9 × 92.4 × 175.6 Å^3. The box was filled with TIP3P water molecules and neutralized with the addition of 27 Na^+ and 15 Cl^- ions respectively, to approximate a 0.1 mM ion concentration. The minimum distance of any protein atom to the edges of the simulation box was 17 Å in order to avoid simulation artifacts [24]. Total number of atoms of the whole system was 131 408.

Non-bonded van der Waals interactions were gradually turned off at a distance between 10 and 12 Å [25]. Long range electrostatics were calculated with the PME method [26]. Non-bonded forces and PME electrostatics were computed every second step. Pair list was updated every 10 steps. Bonds to hydrogen atoms were constrained with the SHAKE method [27] allowing a 2 fs time step for integration. Each system was initially subjected to energy minimization with 5000 steps. The temperature of the system was then gradually increased to 310 K, with Langevin dynamics using the NVT ensemble, during a period of 3000 steps, by stepwise reassignment of velocities every 500 steps. The simulation was continued at 310 K for 200 000 steps (400 ps). During minimization and equilibration phases, protein backbone atoms (N, C^α, C′, O) were restrained to their initial positions with a force constant of 50 kcal mol^{-1} Å^{-2}. The system was equilibrated for another 400 ps with the force constant reduced to 5 kcal mol^{-1} Å^2. Finally, 400 ps of NVT simulation at 310 K was performed with total elimination of the positional restraints. The simulations were passed to the productive phase, by applying constant pressure with the Langevin piston method [28]. Pressure was maintained at 1 atm and temperature at 310 K. Results are based to a period of 20 ns of these isothermal-isobaric (NPT) runs. Snapshots were saved to disk at 1 ps interval for further structural analysis.

Table 1
Backbone dihedral angles of the peptide in tpep and cpep trajectories. The values observed in X-ray structures (PDB codes 3dxa and 3dx8, respectively) are also listed as a reference. Parentheses indicate the estimated standard deviations with the Yamartino method (see Section 2 for details).

Dihedral	PDB		MD	
	tpep	cpep	tpep	cpep
Glu_2 ϕ	−79.9	−90.9	−93.8 (14.9)	−101.7 (13.6)
Glu_2 ψ	164.6	169.7	176.4 (8.3)	168.9 (10.9)
Asn_3 ϕ	−90.6	−126.5	−83.6 (11.3)	−90.2 (16.0)
Asn_3 ψ	126.6	117.6	149.6 (11.6)	96.4 (20.9)
Leu_4 ϕ	−95.6	−109.9	−97.4 (12.5)	−124.3 (16.5)
Leu_4 ψ	86.9	136.7	107.1 (26.4)	121.2 (13.7)
Leu_5 ϕ	−84.1	−70.9	−100.0 (15.3)	−75.3 (12.1)
Leu_5 ψ	125.1	−70.6	88.6 (20.2)	−55.3 (8.3)
Asp_6 ϕ	−84.9	−105.6	−83.8 (15.6)	−88.7 (9.7)
Asp_6 ψ	125.9	−35.3	−77.7 (15.6)	−21.8 (11.3)
Phe_7 ϕ	57.2	−53.5	−107.3 (17.3)	−69.8 (10.3)
Phe_7 ψ	26.8	4.7	40.6 (26.0)	52.3 (12.8)
Val_8 ϕ	−85.7	−67.6	−92.6 (16.6)	−97.4 (13.4)
Val_8 ψ	118.1	113.7	86.4 (15.3)	83.9 (15.3)
Arg_9 ϕ	−148.0	−143.3	−117.5 (15.0)	−106.7 (14.0)
Arg_9 ψ	156.6	153.1	155.9 (14.1)	122.5 (15.2)

2.2. Trajectory analysis

Trajectory analysis of backbone dihedral angles, non-bonded interactions, etc., was performed with the Eucb [29,30] software package. β-Turn classifications were based on geometrical characteristics of the backbone conformation [31]. Initially, a β-turn was accepted if $d(C_i^\alpha - C_{i+3}^\alpha) \leqslant 7$ Å and $|\alpha(C_i^\alpha - C_{i+1}^\alpha - C_{i+2}^\alpha - C_{i+3}^\alpha)| < 90^\circ$, where d is the distance and α is the dihedral angle between the corresponding atoms. Further classification of the β-turn was based on hydrogen bond patterns and backbone dihedral values of the $i+1$ and $i+2$ residues. Appropriate corrections have been taken into consideration for the calculation of angular/circular statistics [32,33]. Secondary structure analysis was performed with STRIDE [34]. Structural figures were prepared with PyMOL (http://www.pymol.org).

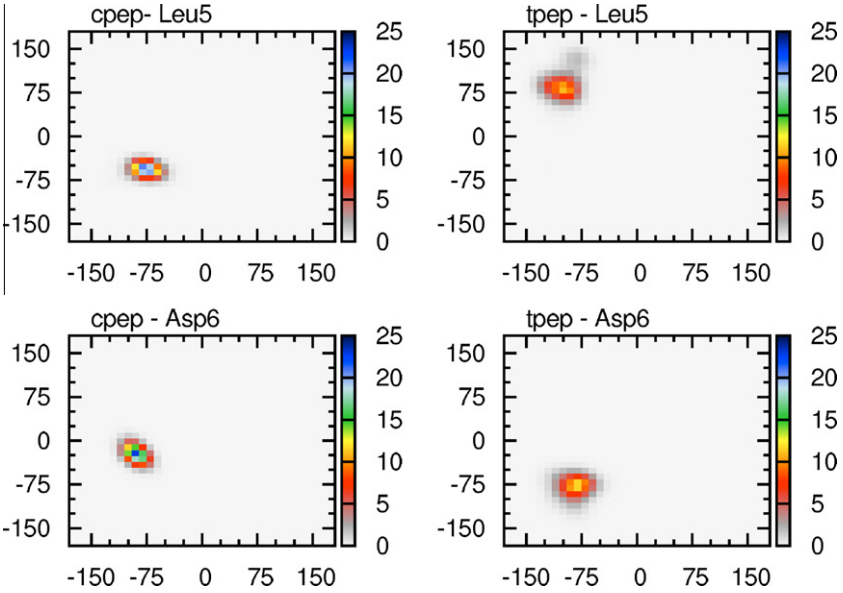

Fig. 2. Ramachandran maps of the backbone dihedral angles (ϕ, ψ) of the Leu5-Asp6 region of the peptide. The maps obtained from the pMHC/TCR trajectory are plotted in the right column, while the maps obtained from the left column are plotted in the left column. Dihedral data values have been extracted for 20 000 frames of the trajectories and they have been binned every 10°. Backbone dihedral angle ψ is plotted horizontally while dihedral angle ψ is plotted vertically. The color sidebar indicates the percentage of frames in each bin.

2.3. Dihedral principal components analysis

Dihedral principal components analysis [35,36] of the peptide was performed with the Carma [37] software package.

2.4. MM-PBSA calculation of $\Delta G_{binding}$

The binding free energy of the association of two molecules (A + B → AB) can be estimated, according to the MM-PBSA approach [38,39]. In the current study, the last 10 ns were used for obtaining trajectory averages, assuming that equilibrium was reached after the first 10 ns of the simulation. 10000 structures were utilized for the calculation of SASA and molecular mechanics calculations, while 50 structures (one every 200 frames) were used for the calculation of the G^{elec}_{solv} with the APBS [40,41] software. Entropy terms were not included in the current calculations.

3. Results

3.1. Backbone dynamics of the peptide

Root mean square fluctuation (RMSF) of C^{α} atoms during MD trajectories and time evolution of root mean square deviation (RMSD) of backbone atoms (N, C^{α}, C′) are presented in Fig. 1. In general, it can be seen that both trajectories were quite stable during the 20 ns of molecular dynamics simulations.

All protein chains in the TCR–HLA^{cpep} complex showed lower RMSD values than the TCR–HLA^{tpep} complex. The difference, as it is revealed form the time evolution plots was approximately 1 Å. The value itself is not that big. However, the fact that the peptide, the MHC molecule and TCR, all showed as increased flexibility in the TCR–HLA^{tpep} is notable. Since the difference between the two simulated complexes was only a *cis*/*trans* peptide bond at the Leu5-Asp6 region then the observed increased flexibility in the TCR–HLA^{tpep} can be ascribed to this conformational transition.

Table 1 lists the values of backbone dihedral angles of residues 2–9 of the peptide, observed in the X-ray structures, as well as the corresponding average values from the TCR–HLA^{cpep} and TCR–HLA^{cpep} trajectories. A notable difference in peptide's backbone dihedral angles is the opposite sign of the ψ dihedral angle of residue Leu5. The corresponding value averaged at 88.6° and −55.3° during the TCR–HLA^{cpep} and TCR–HLA^{tpep}. Thus, differences of approximately 145° have been recorded, indicating a major conformational difference in this region of the peptide. The corresponding difference in the X-ray structure is 175°. The difference in backbone dihedral angles around the Leu5-Asp6 region is highlighted in Fig. 2.

The most striking feature of the backbone's conformational transition after the TCR binding of the pMHC binding was the *cis* peptide bond observed in pMHC/TCR structure, at position Leu5-Asp6 (PDB code 3dxa). The same peptide bond was found in *trans* isomerization state in pMHC complex (PDB code 3dx8). This is the first observation of such an isomerization in peptide's structure after TCR binding of a pMHC complex, and its occurrence must be noted. However, this can not be generalized as a global property of the DM1 T-cell receptor. Most likely, this is an allele dependent feature [14]. Fig. 3 show the probability density of the Leu_5 ω angle with values obtained from the pMHC and pMHC/TCR trajectories. As it can be expected, the ω angle did not show any transition. Non-proline *cis* peptide bonds are relatively rare in proteins and peptides [5]. Moreover *cis* peptide bonds in Leu-Asp fragments are particularly rare [3]. From this point of view, the *cis–trans* isomerization of the Leu5-Asp6 peptide bond is rather unexpected, particularly due to the restrained position of the peptide into the MHC's binding groove, which leaves pretty much less space for movement than the free state of the peptide in a solution. Taken into consideration that this region of the peptide lies in the heart of pMHC/TCR interaction [13], the proposition that the TCR is responsible for this isomerization comes out as logical consequence of this interaction. Thus, the T-cell receptor can only be adapted on the pMHC interface, but it can trigger major conformational transitions at the binding interface.

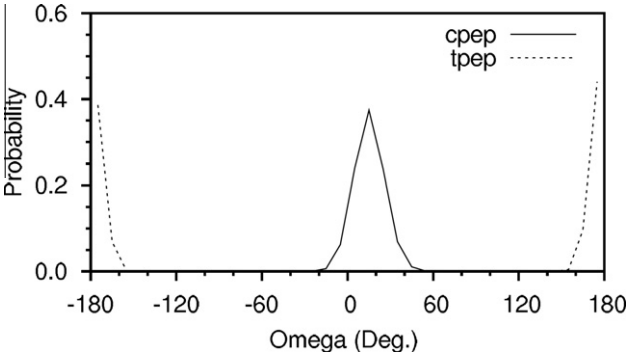

Fig. 3. Probability density plot of the Leu5 ω angle of the peptide in cpep and tpep trajectories.

Analysis of the secondary structure of the peptide's structure with the STRIDE program [34] revealed that the peptide remained in β-turn conformational state in the Leu_5-Val_8 region. Although this β-turn was not accompanied by a stabilizing hydrogen bond (type IV turn), it is proposed that the term "turn" to be used instead of the "bulged" conformation, as this secondary structure plays important role in peptide's recognition in immunological complexes [42,43]. The β-turn remained in presence for approximately 95% of the trajectory frames in both pMHC/TCR complexes.

3.2. Dihedral angle principal component analysis

Dihedral angle principal component analysis has been applied in order to explore the energy landscape of the peptide in TCR–HLA^{cpep} TCR–HLA^{tpep} complexes. Fig. 4 shows the projection of the backbone dihedral angles of the peptide on the planes of the first three principal components. The main difference between the two complexes is that in the TCR–HLA^{cpep} case a dominant conformation can be observed, which is not the case in the TCR–HLA^{tpep} trajectory. A sufficient sampled single-stated structure should lead (in such projections) in a two dimensional Gaussian-type graph, centered at the origin. This is pretty much what one can observe in the TCR–HLA^{cpep} case. However, the TCR–HLA^{tpep} trajectory (bottom row) deviates significantly from this representation. It is clearly stated that the peptide sampled two to three distinct conformational states that differed form those of the TCR–HLA^{cpep} trajectory. These projections corroborate the previously analyzed Ramachandran maps and backbone dihedral angle analysis of the peptide in the TCR–HLA^{cpep} and TCR–HLA^{tpep} complexes respectively.

3.3. Interactions at the pMHC/TCR interface

Fig. 5 show the time evolution between the number of hydrogen bonds between various parts of the molecular complexes. As it can be seen from this figure the interactions between MHC chain α and TCR chains α, β (parts (A) and (B), respectively) are approximately the same. Interestingly, during the second part of the trajectory, the number of hydrogen bonds in TCR–HLA^{tpep} complex exceeded slightly the corresponding number of the TCR–HLA^{cpep} complex. What really different between the two complexes was the number of hydrogen bond interactions between the

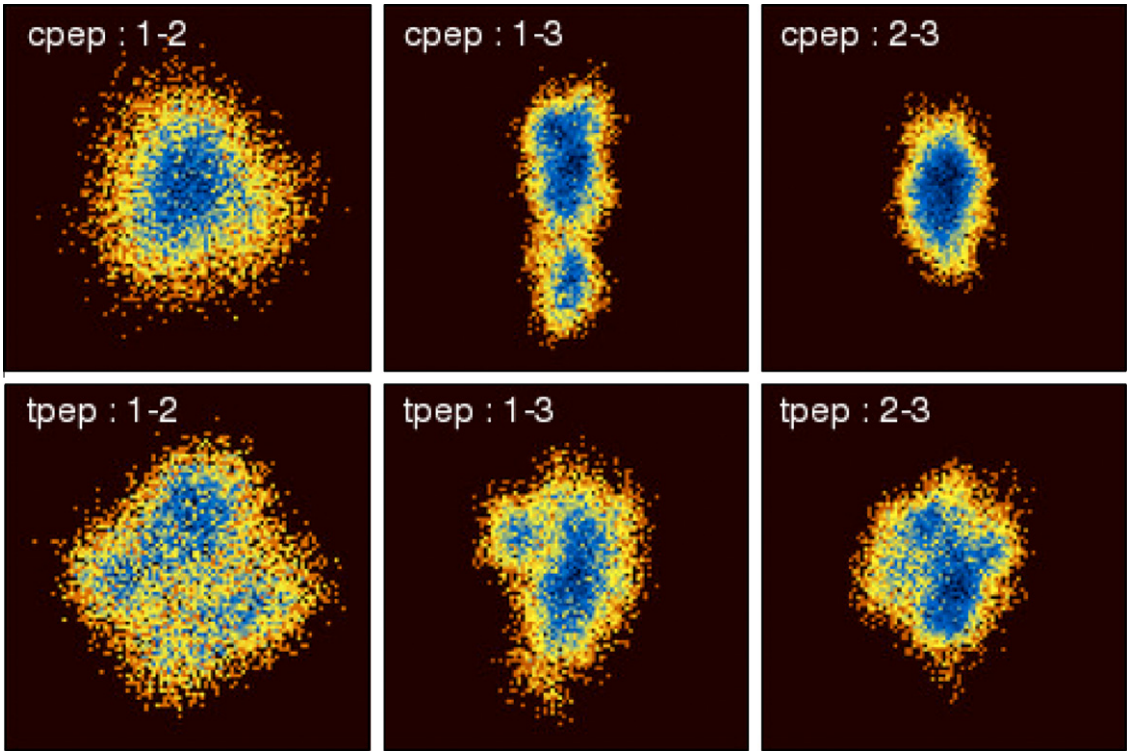

Fig. 4. Dihedral principal component analysis of the peptide. All diagrams shown in this figure are pseudo-color representations of density functions corresponding to the projections of the fluctuations of the peptides backbone dihedral angles (ϕ, ψ) on the planes of the top three eigenvectors. The density function shown is $\Delta G = -k_B T \ln(p/p_{max})$ where k_B is the Boltzmann constant, T is the temperature in Kelvin, and p and p_{max} are probabilities obtained from the distribution of the principal components for each structure (frame) from the corresponding trajectory. The ΔG values obtained from this procedure are on an arbitrary scale in the sense that they depend on the binning procedure used for calculating the p and p_{max} values. For all diagrams of this figure, the raw data were binned on a square matrix of size $N/2$, where N is the number of frames of the corresponding trajectory.

peptide and the and α, β chains of the TCR (parts (C) and (D) of Fig. 5, respectively.) Thus, while the TCR–HLA^{cpep} complex showed remarkably constant hydrogen bond interactions, the TCR–HLA^{tpep} complex exhibited a gradual loss of hydrogen bond interactions between the peptide and the TCR. This fact was observed for both chains of TCR. Approximately 3–4 hydrogen bonds were lost from peptide/TCRα and peptide/TCRβ interfaces. Although the time scale of this simulation work might not be long enough to address the full dynamics of such a big protein complex, the trend in destruction of the hydrogen bond network is clearly and undoubtedly observed.

Taking all of these interactions additively, one can lead to part (E) of Fig. 5, where the total number of hydrogen bond interactions are plotted against simulation time. The difference in this number between the TCR–HLA^{cpep} and TCR–HLA^{tpep} complexes is also highlighted (green dashed line).

Another indication of the instability of the pMHC/TCR interaction in the TCR–HLA^{tpep} complex comes from the hydration of the peptide. Although, the resolution (3.5 Å) of the original complex did not allow the identification of water molecules in the X-ray structure, the evidence provided here corroborates the hypothesis that the TCR–HLA^{tpep} is relatively unstable in comparison with the TCR–HLA^{cpep} complex. Part (F) of the Fig. 5 displays the time evolution of the hydrogen bonds between peptide residues in the region Glu2-Arg9. N- and C-terminus residues were excluded from the current analysis due to their proximity with the bulk solvent. The time series of this quantity was found pretty stable in the TCR–HLA^{cpep} complex, but it showed a constant slight increase over simulation time. The increased hydration of the peptide, which lies in the heart of pMHC/TCR interaction interface, is strongly indicative of the destruction of this interface. The peptide prefers the solvent interaction, which leads to a loss of the binding interface. This observation is in line with the results discussed in the previously, where the decrease in pMHC/TCR interactions were shown.

3.4. Buried surface area analysis

The loss in hydrogen bond interaction contacts can be pretty well summarized by plotting the buried surface are between the pMHC and TCR parts of the TCR–HLA^{cpep} and TCR–HLA^{tpep} complexes, as it is shown in the Fig. 6. Both complexes, exhibited approximately the same BSA value during the first part of the simulation. However, the BSA time series significantly diverged in the TCR–HLA^{cpep} and TCR–HLA^{tpep} cases during the second part. The loss of the BSA, which is directly connected to the binding strength, in remarkable agreement with the loss of the hydrogen bond interactions and the hydration of the peptide in the TCR–HLA^{tpep} case. Thus, accumulated evidence is provided that the TCR–HLA^{tpep} complex is relatively unstable and that DM1 TCR prefers to bind the HLA-B44–peptide complex with the Leu5-Asp6 peptide bond in the *cis* conformation.

3.5. Energetic analysis of pMHC/TCR interactions

The structural observations of the instability of the TCR–HLA^{tpep} are very well reflected in the energetic analysis of the complexes. Computation of the AG_{bind} of the pMHC/TCR complexes with the mm-pbsa method revealed the value of -188.3 kcal mol^{-1} in the TCR–HLA^{tpep}. The corresponding value of the TCR–HLA^{cpep} was found -229.3 -188.3 kcal mol^{-1}. Although the accuracy of the these values can be disputed, the trend is in perfect agreement

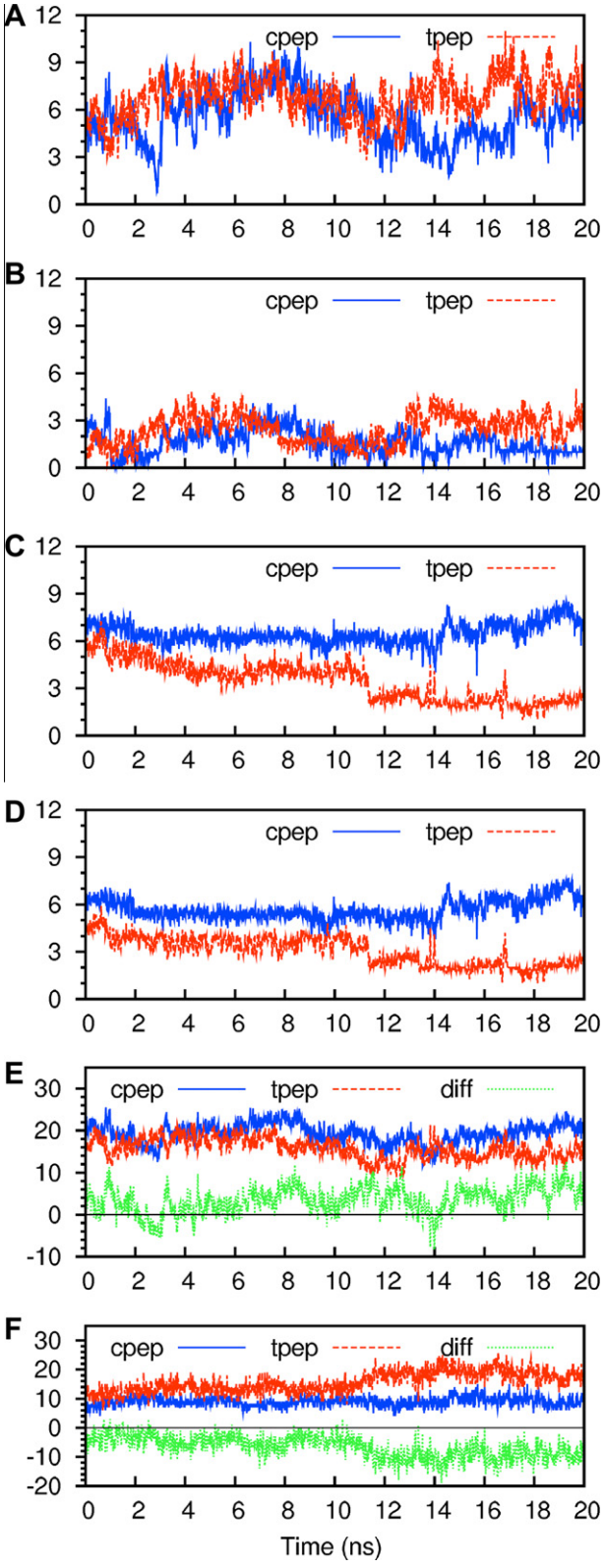

Fig. 5. Hydrogen bond interactions at the pMHC/TCR interface. Time series of total number of hydrgen bonds found in: (A) between MHC chain α and TCR chain α, (B) between MHC chain α and TCR chain β, (C) between peptide α and TCR chain α, (D) between peptide and TCR chain β, (E) between pMHC and TCR, the green line also indicates the difference found between the TCR–HLA^{cpep} and TCR–HLA^{tpep} trajectories, (F) between the peptide (residues 2–9) and water molecules, the green line also indicates the difference found between the TCR–HLA^{cpep} and TCR–HLA^{tpep} trajectories.

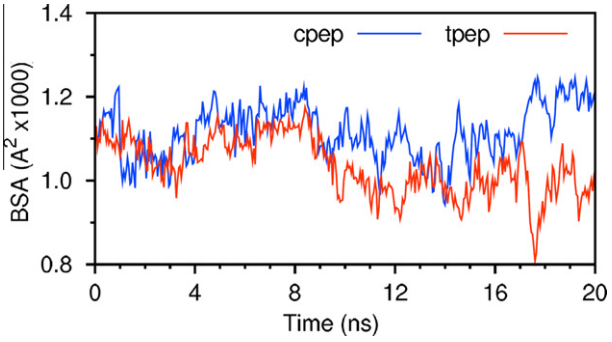

Fig. 6. Buried surface area time evolution in TCR–HLA^{cpep} and TCR–HLA^{tpep} MD trajectories, of pMHC/TCR interface.

with the structural observations and reveals again the preference of DM1 TCR for the *cis* peptide bond conformation in the pMHC complex.

4. Discussion

Cis–trans isomerization of the bound peptide in pMHC/TCR complexes is a rare phenomenon, that is presented here for the first time. Based on TCR–HLA-B*4405^{EENLLDFVRF} and HLA-B*4405^{EENLLDFVRF} X-ray structures, two 20 ns molecular dynamics trajectories have been employed, in order to elucidate the structural and energetic features of this conformational transition. Despite the energetic cost of *cis–trans* isomerization, the T-cell receptor can introduce such a conformational transition to a peptide bound to HLA-B*4405 molecule.

Energetic analysis of the two complexes revealed some interesting features about the preference of the DM1 TCR for a pMHC complex with the Leu5-Asp6 peptide bond in *cis* conformation. The ΔG_{bind} has been found considerably lower in TCR–HLA^{cpep} than in TCR–HLA^{tpep} complex respectively. A single dihedral angle differentiation is a small variation in a complex of 825 residues, however, it effects critically the energetics of binding between the TCR and pMHC complex. The findings from MM-PBSA results are consistent with three other critical facts: (a) the decrease in the buried surface are at pMHC/TCR interface, (b) the decrease in hydrogen bond interactions between pMHC/TCR interface and (c) the significant increase in the hydration of the peptide. All these factors corroborate the hypothesis the TCR–HLA^{tpep} complex is relatively unstable and that the *cis* peptide bond in the Leu5-Asp6 region in the energetically favourable conformation of the peptide in the pMHC/TCR complex. The presence of a relatively rigid conformation of the peptide in TCR–HLA^{cpep} complex is also consistent with a more favourable interaction mode. The *cis* isomerization state of the Leu5-Asp6 bond in pMHC/TCR complex was also accompanied by a beta-turn formation in the Leu5-Val8 region.

Acknowledgements

I thank two anonymous reviewers for their helpfull comments and suggestions. Parallel execution of NAMD was performed at the Research Center for Scientific Simulations (RCSS) of the University of Ioannina. The open source community (Linux, NAMD, GNU, etc.) is gratefully acknowledged for public release of all the necessary computer software needed for this research work.

References

[1] Grünberg, R., Nilges, M. and Leckner, J. (2006) Flexibility and conformational entropy in protein–protein binding. Structure 14, 683–693.

[2] Stavrakoudis, A. (2010) Conformational flexibility in designing peptides for immunology: the molecular dynamics approach. Curr. Comput. Aided Drug Des. 6, 207–222.

[3] Pal, D. and Chakrabarti, P. (1999) *Cis* peptide bonds in proteins: residues involved, their conformations, interactions and locations. J. Mol. Biol. 294, 271–288.

[4] Lu, K.P., Finn, G., Lee, T.H. and Nicholson, L.K. (2007) Prolyl *cis–trans* isomerization as a molecular timer. Nat. Chem. Biol. 3, 619–629.

[5] Jabs, A., Weiss, M. and Hilgenfeld, R. (1999) Non-proline *cis* peptide bonds in proteins. J. Mol. Biol. 286, 291–304.

[6] Lummis, S.C.R., Beene, D.L., Lee, L.W., Lester, H.A., Broadhurst, R.W. and Dougherty, D.A. (2005) *Cis–trans* isomerization at a proline opens the pore of a neurotransmittergated ion channel. Nature 438, 248–252.

[7] Tsikaris, V., Sakarellos-Daitsiotis, M., Tzovaras, D., Sakarellos, C., Orlewski, P., Cung, M. and Marraud, M. (1996) Isomerization of the Xaa-Pro peptide bond induced by ionic interactions of arginine. Biopolymers 38, 673–682.

[8] Güothel, S.F. and Marahiel, M.A. (1999) Peptidyl-prolyl *cis–trans* isomerases, a superfamily of ubiquitous folding catalysts. Cell. Mol. Life Sci. 55, 423–436.

[9] Phan-Chan-Du, A., Hemmerlin, C., Krikorian, D., Sakarellos-Daitsiotis, M., Tsikaris, V., Sakarellos, C., Marinou, M., Thureau, A., Cung, M.T. and Tzartos, S.J. (2003) Solution conformation of the antibody-bound tyrosine phosphorylation site of the nicotinic acetylcholine receptor β-subunit in its phosphorylated and nonphosphorylated states. Biochemistry 42, 7371–7380.

[10] Tugarinov, V., Zvi, A., Levy, R. and Anglister, J. (1999) A *cis* proline turn linking two β-hairpin strands in the solution structure of an antibody-bound HIV-1IIIB V3 peptide. Nat. Struct. Mol. Biol. 6, 331–335.

[11] Madden, D.R., Garboczi, D.N. and Wiley, D.C. (1993) The antigenic identity of peptide–MHC complexes: a comparison of the conformations of five viral peptides presented by HLA-A2. Cell 75, 693–708.

[12] Bui, H.H., Schiewe, A.J., von Grafenstein, H. and Haworth, I.S. (2006) Structural prediction of peptides binding to MHC class I molecules. Proteins: Struct. Funct. Bioinform. 63, 43–52.

[13] Archbold, J.K., Macdonald, W.A., Gras, S., Ely, L.K., Miles, J.J., Bell, M.J., Brennan, R.M., Beddoe, T., Wilce, M.C.J., Clements, C.S., Purcell, A.W., McCluskey, J., Burrows, S.R. and Rossjohn, J. (2009) Natural micropolymorphism in human leukocyte antigens provides a basis for genetic control of antigen recognition. J. Exp. Med. 206, 209–219.

[14] Marrack, P., Scott-Browne, J.P., Dai, S., Gapin, L. and Kappler, J.W. (2008) Evolutionarily conserved amino acids that control TCR-MHC interaction. Ann. Rev. Immunol. 26, 171–203.

[15] Kaas, Q. and Lefranc, M.P. (2005) T cell receptor/peptide/MHC molecular characterization and standardized pMHC contact sites in IMGT/3Dstructure-DB. In Silico Biol. 5, 505–528.

[16] Morikis, D. and Lambris, J.D. (2004) Physical methods for structure, dynamics and binding in immunological research. Trends Immunol. 25, 700–707.

[17] Mallik, B. and Morikis, D. (2006) Applications of molecular dynamics simulations in immunology: a useful computational method in aiding vaccine design. Curr. Proteom. 3, 259–270.

[18] van Gunsteren, W.F., Dolenc, J. and Mark, A.E. (2008) Molecular simulation as an aid to experimentalists. Curr. Opin. Struct. Biol. 18, 149–153.

[19] Flower, D.R., Phadwal, K., Macdonald, I.K., Coveney, P., Davies, M.N. and Wan, S. (2010) T-cell epitope prediction and immune complex simulation using molecular dynamics: state of the art and persisting challenges. Immunome Res. 6, S4.

[20] Berman, H.M., Battistuz, T., Bhat, T.N., Bluhm, W.F., Bourne, P.E., Burkhardt, K., Feng, Z., Gilliland, G.L., Iype, L., Jain, S., Fagan, P., Marvin, J., Padilla, D., Ravichandran, V., Schneider, B., Thanki, N., Weissig, H., Westbrook, J.D. and Zardecki, C. (2002) The protein data bank. Acta Crystallogr. D: Biol. Crystallogr. 58, 899–907.

[21] Feller, S.E. and MacKerell Jr., A.D. (2000) An improved empirical potential energy function for molecular simulations of phospholipids. J. Chem. Phys. B 104, 7510–7515.

[22] Humphrey, W., Dalke, A. and Schulten, K. (1996) VMD: Visual molecular dynamics. J. Mol. Graph. 14, 33–38.

[23] Word, J.M., Lovell, S.C., Richardson, J.S. and Richardson, D.C. (1999) Asparagine and glutamine: using hydrogen atom contacts in the choice of side-chain amide orientation. J. Mol. Biol. 285, 1735–1747.

[24] Weber, W., Hunenberger, P.H. and McCammon, J.A. (2000) Molecular dynamics simulations of a polyalanine octapeptide under Ewald boundary conditions: influence of artificial periodicity on peptide conformation. J. Phys. Chem. B 104, 3668–3675.

[25] Yonetani, Y. (2006) Liquid water simulation: a critical examination of cutoff length. J. Chem. Phys. 124, 204501.

[26] Darden, T., York, D. and Pedersen, L. (1993) Particle mesh ewald: an N log(N) method for Ewald sums in large systems. J. Chem. Phys. 98, 10089–10092.

[27] Ryckaert, J.P., Ciccotti, G. and Berendsen, H.J.C. (1977) Numerical integration of the Cartesian equations of motion of a system with constraints: molecular dynamics of *n*-alkanes. J. Comput. Phys. 23, 327–341.

[28] Feller, S.E., Zhang, Y., Pastor, R.W. and Brooks, B.R. (1995) Constant pressure molecular dynamics simulation: the Langevin piston method. J. Chem. Phys. B 103, 4613–4621.

[29] Tsoulos, I.G. and Stavrakoudis, A. (2011) Eucb: a C++ program for molecular dynamics trajectory analysis. Comput. Phys. Commun. 182, 834–841.

[30] Stavrakoudis, A. (2009) A disulfide linked model of the complement protein C8γ complexed with C8α indel peptide. J. Mol. Model. 15, 165–171.

[31] Hutchinson, E.G. and Thornton, J.M. (1994) A revised set of potentials for beta-turn formation in proteins. Protein Sci. 3, 2207–22016.

[32] Döker, R., Maurer, T., Kremer, W., Neidig, K. and Kalbitzer, H.R. (1999) Determination of mean and standard deviation of dihedral angles. Biochem. Biophys. Res. Commun. 257, 348–350.

[33] Yamartino, R.J. (1984) A comparison of several "single-pass" estimators of the standard deviation of wind direction. J. Climate Appl. Meteorol. 23, 1362–1366.

[34] Frishman, D. and Argos, P. (1995) Knowledge-based protein secondary structure assignment, proteins: structure. Funct. Genet. 23, 566–579.

[35] Maisuradze, G.G., Liwo, A. and Scheraga, H.A. (2009) Principal component analysis for protein folding dynamics. J. Mol. Biol. 385, 312–329.

[36] Mu, Y., Nguyen, P.H. and Stock, G. (2005) Energy landscape of a small peptide revealed by dihedral angle principal component analysis. Proteins: Struct. Funct. Bioinform. 58, 45–52.

[37] Glykos, N.M. (2006) Carma: a molecular dynamics analysis program. J. Comput. Chem. 27, 1765–1768.

[38] Kollman, P., Massova, I., Reyes, C., Kuhn, B., Huo, S., Chong, L., Lee, M., Lee, T., Duan, Y., Wang, W., Donini, O., Cieplak, P., Srinivasan, J., Case, D.A. and C.T.E. (2000) Calculating structures and free energies of complex molecules: combining molecular mechanics and continuum models. Acc. Chem. Res. 33, 889–897.

[39] Wan, S., Coveney, P.V. and Flower, D.R. (2005) Peptide recognition by the T cell receptor: comparison of binding free energies from thermodynamic integration, Poisson–Boltzmann and linear interaction energy approximations. Philos. Trans. R. Soc. A 363, 2037–2053.

[40] Baker, N.A., Sept, D., Joseph, S., Holst, M.J. and McCammon, J.A. (2001) Electrostatics of nanosystems: application to microtubules and the ribosome. Proc. Natl. Acad. USA 98, 10037–10041.

[41] Dolinsky, T.J., Nielsen, J.E., McCammon, J.A. and Baker, N.A. (2004) PDB2PQR: an automated pipeline for the setup of Poisson–Boltzmann electrostatics calculations. Nucl. Acids Res. 32, W665–W667.

[42] Tatsis, V.A., Tsoulos, I.G. and Stavrakoudis, A. (2009) Molecular dynamics simulations of the TSSPSAD peptide antigen in free and bound with CAMPATH-1H Fab antibody states: the importance of the β-turn conformation. Int. J. Pept. Res. Ther. 15, 1–9.

[43] Kee, K.S. and Jois, S.D. (2003) Design of beta-turn based therapeutic agents. Curr. Pharm. Des. 15, 1209–1224.